Climate Simulations for 1951–2050 with a Coupled Atmosphere–Ocean Model

SHAN SUN AND JAMES E. HANSEN

NASA Goddard Institute for Space Studies, New York, New York

(Manuscript received 9 October 2002, in final form 31 March 2003)

ABSTRACT

The authors simulate climate change for 1951–2050 using the GISS SI2000 atmospheric model coupled to HYCOM, a quasi-isopycnal ocean model (''ocean E''), and contrast the results with those obtained using the same atmosphere coupled to a passive Q-flux ocean model (''ocean B'') and the same atmosphere driven by observed SST (''ocean A''). All of the models give reasonable agreement with observed global temperature change during 1951–2000, but the quasi-isopycnal ocean E mixes heat more deeply and hence sequesters heat more effectively on the century timescale. Global surface warming in the next 50 yr is only 0.3°–0.4°C with this ocean in simulations driven by an ''alternative scenario'' climate forcing (1.1 W m^{-2} in the next 50 yr), only half as much as with ocean B. From the different models the authors estimate that the earth was out of radiation balance by about 0.18 W m^{-2} in 1951 and is now out of balance by about 0.75 W m^{-2}. This energy imbalance, or residual climate forcing, a consequence of deep ocean mixing of heat anomalies and the history of climate forcings, is a crucial measure of the state of the climate system that should be precisely monitored with full-ocean temperature measurements.

1. Introduction

Global surface air temperature has increased about 3/4°C since the late 1800s (Jones et al. 1999; Hansen et al. 2001; Houghton et al. 2001), with most of the warming during the last 50 yr. Although unforced climate fluctuations may contribute to this warming, the recent warming spike is superposed on a cooling trend that had occurred in this millennium (Mann et al. 1998) and indeed upon a longer-term cooling trend since the peak of the current interglacial period (Lamb 1977). There is evidence, reviewed by Houghton et al. (2001), that at least a large part of the recent warming has been driven by external forcings, that is, imposed perturbations of the earth's energy balance. The most prominent forcings in the past century are increasing anthropogenic greenhouse gases (GHGs) and aerosols, although changing solar irradiance also may have contributed significantly (Houghton et al. 2001; Hansen 2000; Shindell et al. 2001a). The GHG climate forcing is the largest, most accurately known forcing. About 70% of the anthropogenic GHG forcing has been introduced since 1950 (Hansen et al. 2002).

Numerous simulations of recent climate change have been carried out with global climate models, including projections into the twenty-first century (Hansen et al. 1988, 1993; Manabe et al. 1991; Cubasch et al. 1992; Meehl et al. 1993; Mitchell et al. 1995; others reviewed by Houghton et al. 1996, 2001). The primary factors influencing the global mean temperature response in these models, and presumably in the real world, are 1) the climate forcings, 2) the equilibrium climate sensitivity, and 3) the effective thermal inertia of the ocean. Our present paper provides a limited investigation of the third factor, the role of the ocean's thermal inertia. Specifically, we examine the role of the ocean representation in determining the transient surface air temperature response to a specified scenario of climate forcings with a climate sensitivity that is nominally fixed.

We simulate the past half-century and the next half-century. The change of climate forcings in the past 50 yr was large and, except for aerosols, the primary forcings are defined reasonably well for that period. The most accurate and complete measurements of climate change are also available for that period. Although earlier initiation of climate simulations would be useful, we have argued that the planet was probably not far out of radiative balance in the 1950s (Hansen et al. 1988). Dixon and Lazante (1999) have shown that global warming and the strength of their modeled oceanic thermohaline circulation in the twenty-first century are insensitive to 1766, 1866, and 1916 choices for model initiation. Given the difficulty in defining earlier climate forcings and our computer limitations, we choose to ''cold start'' our models in 1951 assuming energy balance at that time. This assumption and start date impose limitations that must be recognized in interpreting the results. We view these simulations as an intermediate

Corresponding author address: Dr. Shan Sun, NASA Goddard Institute for Space Studies, 2880 Broadway, New York, NY 10025.
E-mail: ssun@giss.nasa.gov

step between calculations for the post-1979 satellite era (Hansen et al. 1997), for which we included an initial planetary radiation imbalance of 0.65 W m^{-2}, and calculations that begin in the pre-industrial era, when the issue of the initial planetary radiation balance should be practically moot.

2. Atmosphere–ocean models

The principal simulations reported here were carried out with the coupled model described by Sun and Bleck (2001). It consists of the Goddard Institute for Space Studies (GISS) SI2000 atmospheric model (Hansen et al. 2002) with 12 levels in the vertical and a $4° \times 5°$ spherical grid in the horizontal, and the HYCOM ocean model (Bleck and Benjamin, 1993; Bleck 2002), a hybrid coordinate version of the Miami Isopycnal Coordinate Ocean Model (MICOM; Bleck et al. 1992) with 16 vertical layers. ''Hybrid'' here means isopycnal layers in the interior individually connected to constant-z layers near the surface. The horizontal resolution in HYCOM is $2° \times 2°$ cos(latitude) except in the Arctic, where a bipolar projection (Arfken 1970, chapter 2.9) is used that has variable mesh size of no more than 1°. The ocean model is capped by the GISS four-layer thermodynamic ice model (Russell et al. 2000). Diapycnal diffusion in HYCOM is prescribed to be inversely proportional to the buoyancy frequency N: 3×10^{-7} (m^2 s^{-2}) N^{-1}. Constant-z layers are 20 m thick. We call this model ''ocean E.''

We employ two additional ocean representations, oceans A and B, for simulations that can be contrasted with those for ocean E. All three oceans are attached to the same atmospheric model (GISS SI2000) and they are driven by identical climate forcing scenarios.

Ocean A consists of observed SST and sea ice histories for 1951–98 (Rayner et al. 2003), which are imposed as boundary conditions on the atmospheric model. Ocean heat storage in ocean A must be obtained from fluxes at the ocean surface with the assumption that the planet was in radiative balance in 1951, which requires that we subtract from the simulated heat storage a small imbalance calculated for 1951, as discussed in section 6a(1).

Ocean B is the Q-flux model of Hansen et al. (1984), which has specified horizontal heat transports chosen such that the control run nominally reproduces observed SSTs. Temperature anomalies in the climate experiments penetrate the ocean beneath the mixed layer as diffusive tracers with diffusion coefficients based on local climatological column stability. The ocean extends to a depth of 1 km.

Control runs are carried out for each ocean model attached to the SI2000 atmospheric model with the 1951 atmospheric composition specified by Hansen et al. (2002). The purpose of the 20-yr ocean A control run is to obtain a precise measure of the planetary energy imbalance in 1951, as discussed in section 6a. The 100-yr control run for ocean B reveals the model's unforced variability and provides initial conditions for the transient experiments.

The ocean E control run is initiated with the ocean temperature/salinity climatology of Levitus et al. (1994) and Levitus and Boyer (1994). We apply no flux adjustments with ocean E because such nonphysical adjustments can have a significant effect on the simulated climate (Neelin and Dijkstra 1995; Tziperman 2000). The disadvantage is that the model climate has a non-negligible climate drift. The drift of global mean surface air temperature is +0.3° during years 100–200 and +0.05° during years 200–300. By year 300 the model is still out of energy balance by 1.3 W m^{-2}; given the model's sensitivity, inferred in section 5b, this implies that the model would warm about 0.8° if it were run to equilibrium. We deal with the surface temperature drift rate, which is moderate, by differencing experiment and control runs.

Model resolution limits the realism of simulated climate. However, the effective horizontal atmospheric resolution is somewhat higher than the nominal $4° \times 5°$ because of preservation of within-gridbox gradients (Russell and Lerner 1981) using the quadratic upstream differencing scheme (Prather 1986), and in at least some fields the model's fidelity with observations is similar to that of the T42 Max Planck Institute model (Boyle 1998). The coarse vertical resolution and low (10 hPa) rigid lid of the model are a serious limitation, leaving the model unable to realistically simulate stratosphere–troposphere interactions. The 12-layer model (Hansen et al. 2002) does not simulate the observed trend of the Arctic Oscillation, which is captured by versions of the GISS model with better vertical resolution and higher model top (Shindell et al. 2001b). Ocean E horizontal resolution does not resolve the equatorial waveguide, and this probably contributes to the low amplitude of ENSO variability in the model. Other major shortcomings of the atmospheric model that affect the coupled model are 1) deficiency of low-level stratus clouds off the west coast of continents, which causes excessive solar heating of the ocean surface in these regions by as much as 50 W m^{-2}, and 2) deficient wind stress on the ocean surface, which causes coastal upwelling to be too weak. These atmospheric deficiencies are the likely cause of the too-deep tropical thermocline in the east equatorial Pacific in ocean E, which must also contribute to deficient ENSO variability.

Another deficiency in this version of the ocean E coupled model is that the hydrologic cycle is not closed. River runoff is included, but it is deficient by about 0.8 Sv (1 Sv $\equiv 10^6$ m^3 s^{-1}), leading to a salinity drift in the control run, as discussed by Sun and Bleck (2001). Huang et al. (2003) examine several coupled models, including some with significant salinity drift, and in all cases find that the surface heat flux, not the moisture flux, dominates the density flux and ocean heat uptake. Therefore we expect that our experiments were not un-

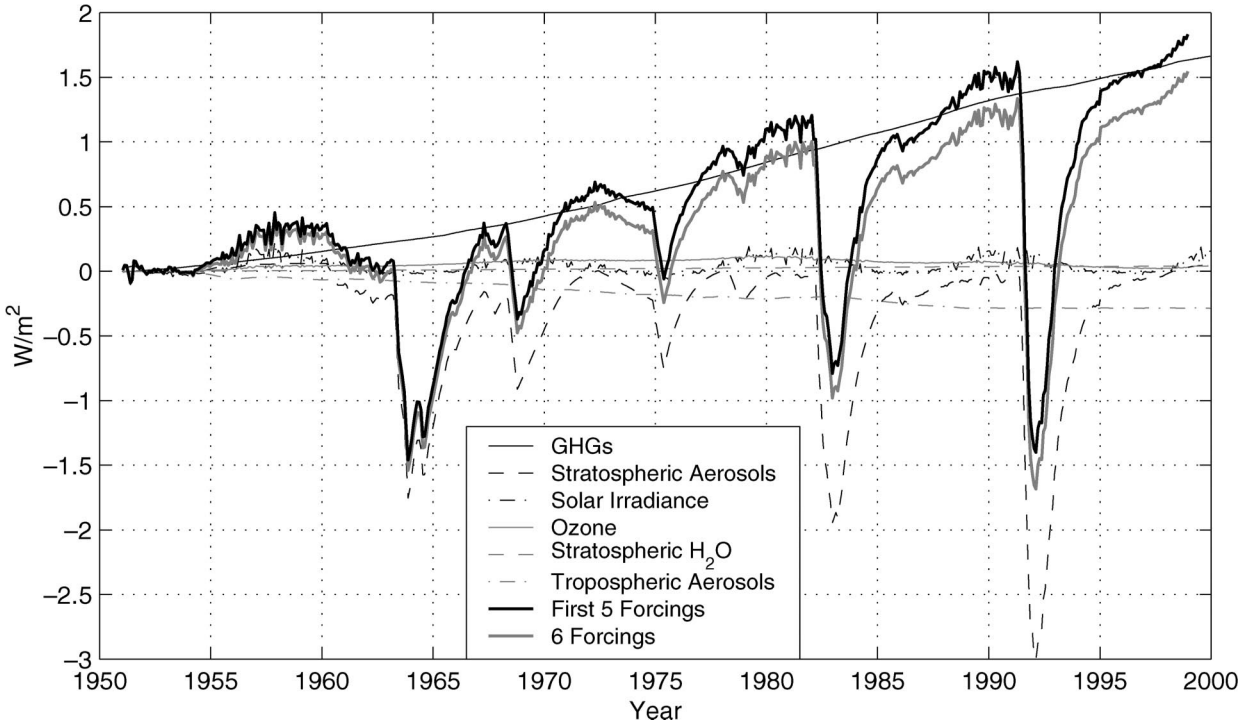

FIG. 1. Global-mean climate forcings employed in transient simulations, from data of Hansen et al. (2002).

duly influenced by this flaw. The flaw is corrected in the 2003 version of the model, which is being used for new simulations.

3. Climate forcings

We employ climate forcings identical to those used by Hansen et al. (2002). During 1951–2000 the forcings are 1) well-mixed GHGs, 2) stratospheric aerosols, 3) solar irradiance, 4) ozone, 5) stratospheric water vapor, and 6) tropospheric aerosols. The global means of these six forcings, and their sum, are shown in Fig. 1. Because the tropospheric aerosol forcing is especially uncertain, we also make simulations with tropospheric aerosols fixed so that they provide zero forcing.

For the period 2000–50 we employ the two scenarios used by Hansen et al. (2002). The ''business-as-usual'' (BAU) scenario, designed to yield a large forcing, has CO_2 increase by 1% yr^{-1}, yielding a forcing of ~2.9 W m^{-2} after 50 yr. The ''alternative'' (ALT) scenario has 1) a CO_2 growth rate in the first two decades of the twenty-first century that is slightly higher than in the last decade of the twentieth century and then a slowly declining growth rate; 2) a CH_4 growth rate that continues to decline slowly such that the absolute CH_4 amount peaks in 2015 before declining slowly; 3) continued N_2O growth throughout the 50 yr, but at a slowly declining rate; 4) a balance between decreasing chlorofluorocarbon and increasing ''other trace gas'' forcings after 2000; and 5) the same sequence of stratospheric aerosol optical depth in 2000–50 as in the previous 50 yr. The 50-yr increase in forcing in the ALT scenario is 1.1 W m^{-2}.

The ALT scenario differs from any of the Houghton et al. (2001) scenarios. Air pollution climate forcings (black carbon, O_3, and CH_4) increase in the Intergovernmental Panel on Climate Change (IPCC) scenarios, while they are flat or declining in the ALT scenario. CO_2 growth in the ALT scenario is about the same as in the slowest growth IPCC scenario.

4. Simulations for 1951–2000

Sun and Bleck (2001) describe the first 200 yr of the coupled model control run. That run has since been extended to 300 yr. We obtain a five-member ensemble of climate change experiments by using the ocean and atmosphere conditions at years 100, 125, 150, 175, and 200 of the control run as the initial conditions and then employing the transient atmospheric forcings for 1951–2000. The modeled climate change was taken to be the difference between the simulated climate and that of the control run for the same period.

a. Simulated climate change

Figure 2 summarizes global temperature changes at three levels in the atmosphere and the global ocean heat storage. We contrast the results of the coupled dynamical atmosphere–ocean model (ocean E) with the results ob-

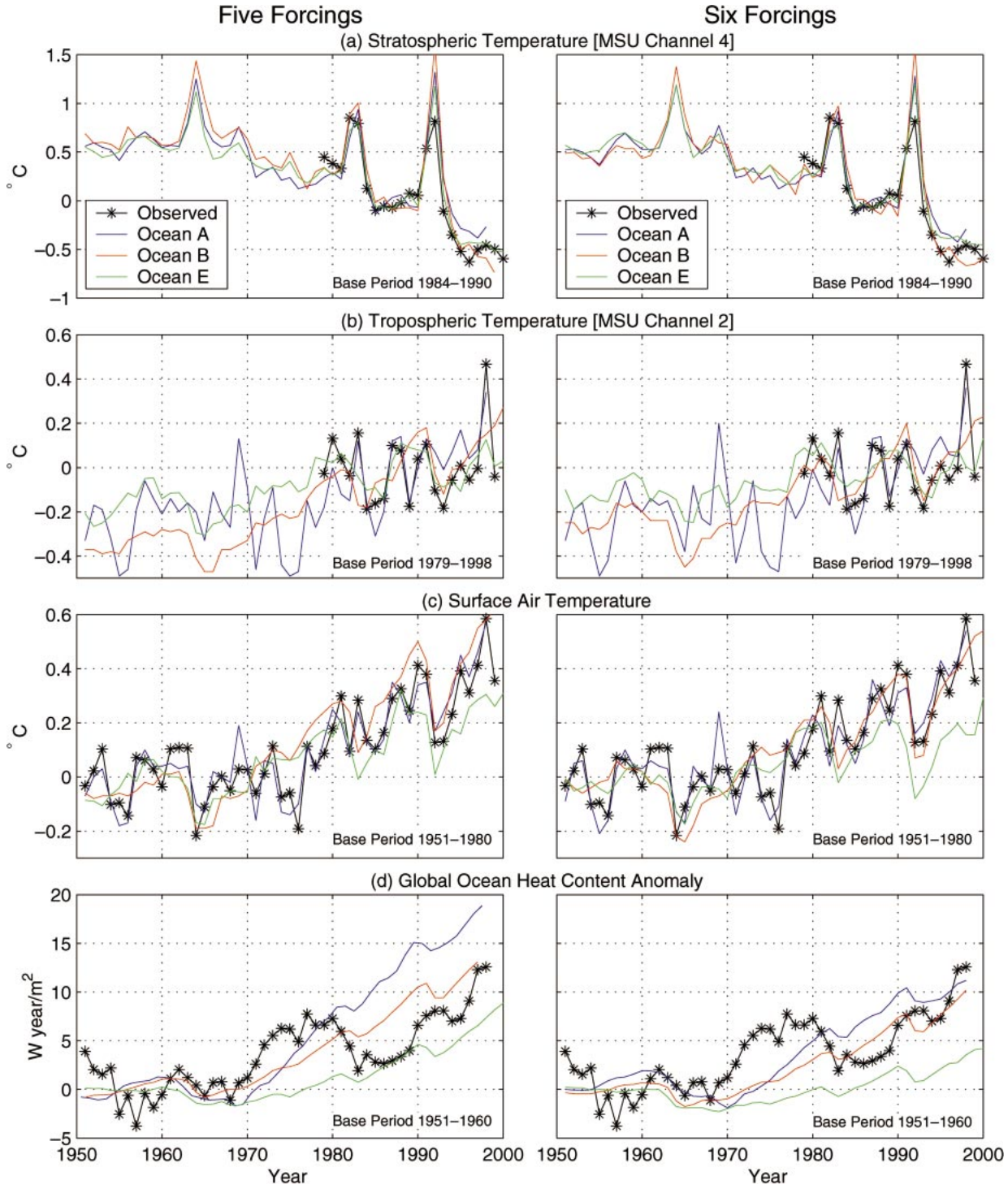

FIG. 2. Transient response of the model for three representations of the ocean. Results on the right employ six forcings, while those on the left exclude tropospheric aerosol changes.

tained by Hansen et al. (2002) using observed SST (ocean A) and the Q-flux ocean (ocean B).

Stratospheric temperature changes over 1951–2000 [with the vertical weighting of the Microwave Sounding Unit (MSU) channel 4], Fig. 2a, do not depend strongly on the ocean representation. Tropospheric temperature changes (Fig. 2b) are flatter (less warming) with ocean E, which is nominally in better agreement with MSU data for the period covered by satellite data. However, we show below that ocean E is not necessarily in better

agreement with radiosonde data over the longer period. The surface air warming (Fig. 2c) and ocean heat storage (Fig. 2d) are smaller with ocean E than with oceans A and B, and also smaller than in observations, especially when one considers ocean E driven by all six forcings.

The smaller surface and tropospheric warming and smaller ocean heat storage in ocean E (HYCOM), compared with ocean B, must be due in part to the smaller equilibrium climate sensitivity[1] of ocean E (~2.4°C for doubled CO_2, compared to 2.8°C for ocean B, as discussed in section 6). Ocean E has less sea ice in its control run (2% of global area) than oceans B and A (4% of global area). Also cloud feedbacks, and thus both the model sensitivity and the heat flux into the ocean, have been shown to depend on the geographical distribution of SST and its changes (Yao and Del Genio 2002). Distinctions between oceans B and E become clearer when the runs are extended to 2050 (section 5). However, we first discuss in greater detail the results for the period with observational data.

The cold start of the model in 1951 probably contributes to the minimal surface warming in the first several decades. Hansen et al. (1988) argue that planetary energy imbalance was probably small in the 1950s, but ~30% of the GHG forcing was introduced prior to 1951, so it is likely that a small positive ''disequilibrium'' forcing (planetary radiation imbalance) existed in 1951. A cold start has less effect on ocean B than on ocean E, because, as we discuss below, the diffusive ocean B does not mix heat as deeply and the near-surface layer responds more rapidly. With improving computational capabilities it should be practical to minimize this issue in future simulations by beginning the runs at an earlier date.

Figure 3 allows a closer comparison of the temperature change versus height for the period of radiosonde data (beginning in 1958) and the period of satellite data (beginning in 1979). The radiosonde data analysis is that of Parker et al. (1997); the alternative version (HadRT2.1) uses MSU data to attempt to correct for bad radiosonde records. Although the radiosonde data are not considered reliable above ~100-hPa level, it appears that the models do not cool the stratosphere as much as observed. As discussed by Hansen et al. (2002), the simulations at these altitudes are affected by uncertainties in the trends of climate forcings, especially ozone and stratospheric water vapor, and even by the trend in the vertical profile of black carbon aerosols. The inclusion of a dynamical ocean (ocean E) does not have a large systematic effect on the simulated stratospheric temperature change.

Ocean E, compared with other ocean representations, has an effect on the simulated temperature change in the troposphere and at the surface. Over the longer period of radiosonde data, ocean E yields less warming than oceans A and B. Over the period of satellite data, ocean E yields almost no tropospheric and surface warming, similar to radiosonde and MSU observations but in contrast to observed surface air warming. Overall, compared with oceans A and B, ocean E yields comparably good agreement with observed global temperature changes.

We caution that, although ocean E yields little tropospheric warming in 1979–98, it does not offer an explanation for the discrepancy between the temperature trends at the surface and in the lower troposphere (Wallace et al. 2000). None of the models yield the observed decrease in the warming trend from the surface to the lower troposphere. There are observational uncertainties in the satellite, radiosonde, and surface data, and, indeed, uncertainty bars on the global data (Fig. 3) suggest no significant discrepancy between the modeled and observed temperature change. However, closer examination reveals some significant discrepancies (Hansen et al. 2002). Hansen et al. (2002) suggest that imprecision in the aerosol and other forcing histories could account for at least part of the discrepancies, but investigation of this topic is beyond the scope of our current paper.

b. Details of ocean heat storage

We examine the ocean heat storage in greater detail for the case of five forcings, because in that case ocean E yields global surface warming comparable to observations. Therefore the ocean heat storage is larger and easier to track amidst the unforced variability of ocean temperature. Although aerosol climate forcing (the sixth forcing) must exist, there is uncertainty in its value as well as that of other forcings, including any forcing due to disequilibrium in 1951, that is, any small planetary radiation imbalance due to the climate forcing history prior to 1951. The difference between the five-forcing and six-forcing scenarios (Fig. 1) is well within the uncertainty in the net forcing as, for example, we have argued that the positive forcings by black carbon and tropospheric ozone may be understated (Hansen et al. 2002). Thus the fact that ocean E requires a greater net forcing than ocean B to match the observed rate of surface warming does not provide an argument against ocean E.

Figure 4a illustrates the variability of global ocean heat storage among the five members of the ensemble of runs with ocean model E. In this case, with five forcings, the modeled heat storage between 1951 and 1998 ranges from 7 to 11 W yr m^{-2} (with six forcings it ranges from 1 to 5 W yr m^{-2}). The Levitus et al. (2000) data yield a heat gain of ~10 W yr m^{-2} between 1951 and 1998, although it is difficult to define the observed change of ocean heat content precisely because of poor spatial sampling in the early 1950s and the large apparent variability in the 1950s. Because of

[1] The equilibrium climate sensitivity is commonly defined by the increase in global mean surface air temperature in response to doubling of atmospheric CO_2 amount, after SST has had time to fully respond to the imposed climate forcing.

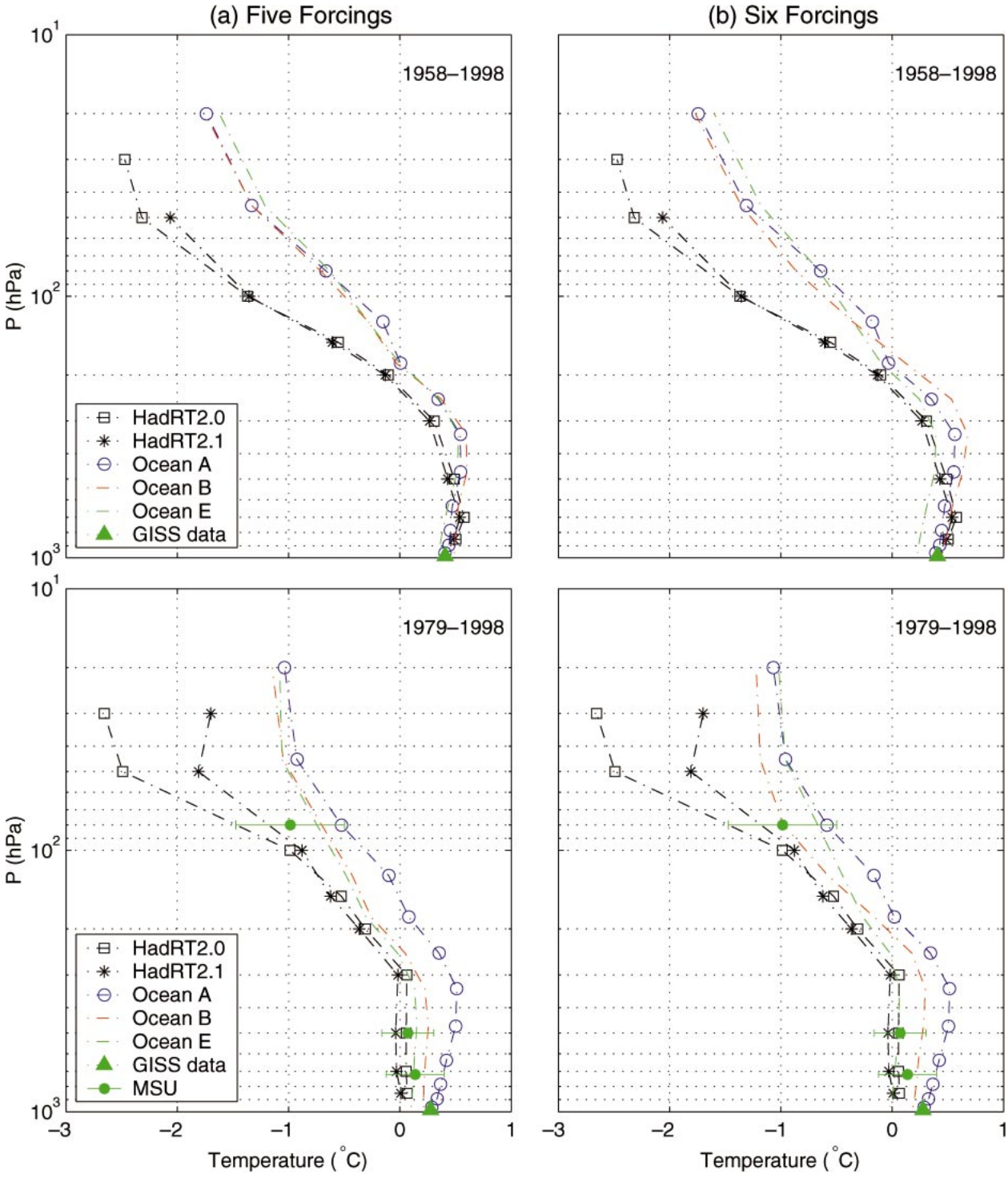

FIG. 3. Global mean annual mean temperature change for (top) 1958–98 and (bottom) 1979–98 based on linear trends. Model results are for oceans A, B, and E with (a) five forcings and (b) six forcings. Radiosonde data become unreliable above ~100 hPa; alternative radiosonde analyses HadRT2.0 and HadRT2.1 are from Parker et al. (1997). The surface observations (green triangles) are the land–ocean data of Hansen et al. (1999) with SST of Reynolds and Smith (1994) for ocean areas. The green bars for MSU satellite data (Christy et al. 2000) are twice the standard statistical error adjusted for autocorrelation (Santer et al. 2000).

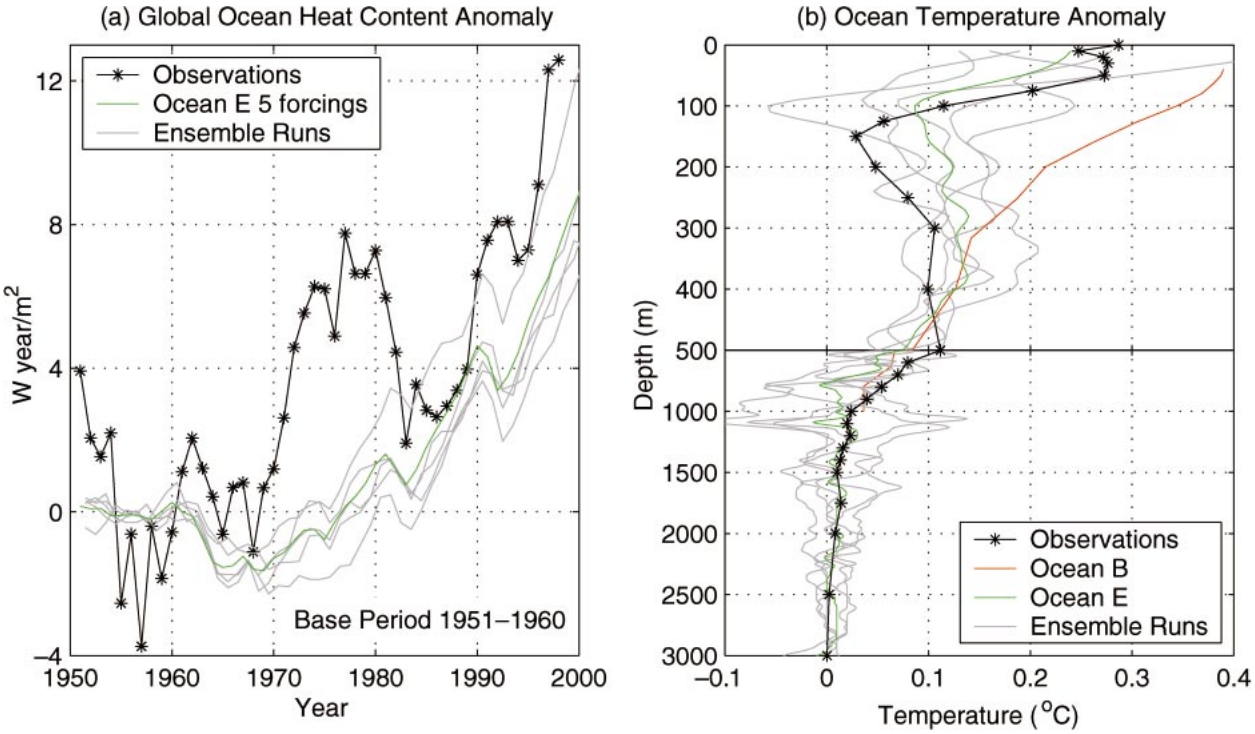

FIG. 4. (a) Global mean ocean heat content anomaly vs time relative to 1951 for Levitus et al. (2000) observations and for the ensemble of runs of ocean E with five climate forcings. (b) Global mean ocean temperature change vs depth between 1951 and 1998 from observations and as simulated with five forcings for ocean B (ensemble mean) and ocean E (ensemble mean and individual runs).

the poor sampling in the early 1950s, Levitus et al. (2000) analyze the heat storage from 1955 onward. Considering the variability in the simulated heat storage from run to run and the fact that the real world only ran through this ''experiment period'' once, we conclude that the model yields reasonable agreement with observed heat storage, at least when the climate forcing in the model is sufficiently large to warm the surface comparable to observations.

We define heat storage as change of the total energy content of the ocean. We evaluate the heat content from the interior ocean temperatures for oceans B and E and observations. For ocean A we calculate the heat storage from the simulated energy fluxes at the ocean surface. Our unit for heat content, W yr m^{-2}, allows direct comparison with the time integral of the climate forcings as defined in Fig. 1.[2] Thus, for example, for our estimated aerosol forcing (Fig. 1), which grows approximately linearly from zero to -0.3 W m^{-2} in 47 yr, the expected change in ocean heat storage is -7 W yr m^{-2}, consistent with the change in heat storage mentioned in the paragraph above.

None of the ensemble members yield decadal variability of ocean heat storage as great as suggested by the Levitus et al. (2000) data. Neither Barnett et al. (2001) nor Levitus et al. (2001) obtained decadal variations in ocean heat storage similar to observations in their climate model simulations, although Barnett et al. (2001) note that they found some decadal variations comparable in magnitude to those observed. It is possible that greater variability would have been obtained in our runs if the ensemble members had not all been initiated within a 100-yr period of the model control run. Another possibility is that the decadal variability in the Levitus et al. (2000) data is an artifact of measurement error and incomplete sampling. Indeed, the results in Fig. 2d for ocean A, in which ocean heat storage is calculated from the modeled surface fluxes for observed ocean temperatures, do not seem to be consistent with the large swings in the observed ocean heat storage, as discussed in sections 6a(2) and 7b.

Figure 4b shows the depth profile of ocean heat storage for the same ensemble of runs as in Fig. 4a. There is substantial variability in the profile of heat storage with ocean E, unlike the diffusive ocean B in which the ocean warming declines monotonically with depth. Indeed, ocean E yields a minimum in ocean warming at ~100 m depth, while the observed profile has a minimum at 150-m depth. One of the ensemble members has cooling at 100 m. The individual model runs exhibit greater variability with depth than the observational analysis. This might be in part a result of implicit smoothing of the observations as a result of interpola-

[2] 1 W yr $\approx 3.15 \times 10^7$ J; so 1 W yr m^{-2} over the entire surface of the earth corresponds to 1.61×10^{22} J.

tions and climatological values employed in data sparse regions (S. Levitus 2002, personal communication). It is partly due to the fact that, because of the model drift, we obtained the heat storage by subtracting the control run, year by year, from the experiment run, thus increasing noise by approximately the square root of 2.

Figure 5 shows the latitude variation of ocean heat storage for the full ocean (top two panels) and for successive layers. Ocean B yields close agreement with the observed full-ocean global mean heat storage over the half-century (10 W yr m^{-2}), although the latitude variations are smoother than observations. Ocean E yields variability of heat storage with latitude comparable to that in observations, although the primary observed feature, the maximum at 0°–30°N, is not captured in its magnitude. Ocean B has no heat storage at depths greater than 1 km, as the ocean bottom was placed at that level. We comment on the zonal mean heat storage in ocean A after presenting the geographical distribution of heat storage in that model.

Figure 6 provides global maps of ocean heat storage between 1951 and 1998, as inferred by Levitus et al. (2000) from ocean temperature observations and as simulated with different representations of the ocean. The calculated heat storage for oceans A and B of course does not include any change in local heat storage due to changes in horizontal ocean heat transport, although with ocean A changes in ocean heat transport that are reflected in the SST may affect the vertical heat exchange at the ocean surface and thus the calculated heat storage. These limitations of oceans A and B are part of the reason that comparison of the sequence of ocean representations is of interest.

The Levitus observational data reveal that the large heat storage at latitudes 0°–30°N (Fig. 5) occurred especially in the Atlantic and eastern Pacific Oceans (Fig. 6). The negative change of heat content in the North Atlantic Ocean, with strong positive values at lower latitudes, suggests some slowing of the meridional circulation over the 47-yr period, but there are not observations of the circulation adequate to verify that inference. There are also regions of large heat storage in a circum-Antarctic belt, although observational data there are limited and thus ocean temperature trends are more uncertain.

The heat storage in ocean A (observed SST) climate simulations has net positive storage in the Atlantic and Pacific Oceans comparable to observations, but the geographical pattern of heat storage in ocean A differs markedly from observations in the Pacific Ocean. This is not surprising as actual regions of heat storage depend in part upon convergence of ocean heat anomalies associated with dynamical fluctuations in ocean transports. For example, waters off the west coast of the United States and Mexico warmed during the past two decades, probably because of increased net ocean heat transport into that region. Associated warm SST anomalies cause the sensible and latent heat fluxes into the atmosphere from that ocean region to increase in the ocean A climate simulations, thus yielding a negative ocean heat content change in that model. Similarly, the Baffin Bay–Greenland Sea region draws extra heat from the atmosphere in ocean A climate simulations because the SST has

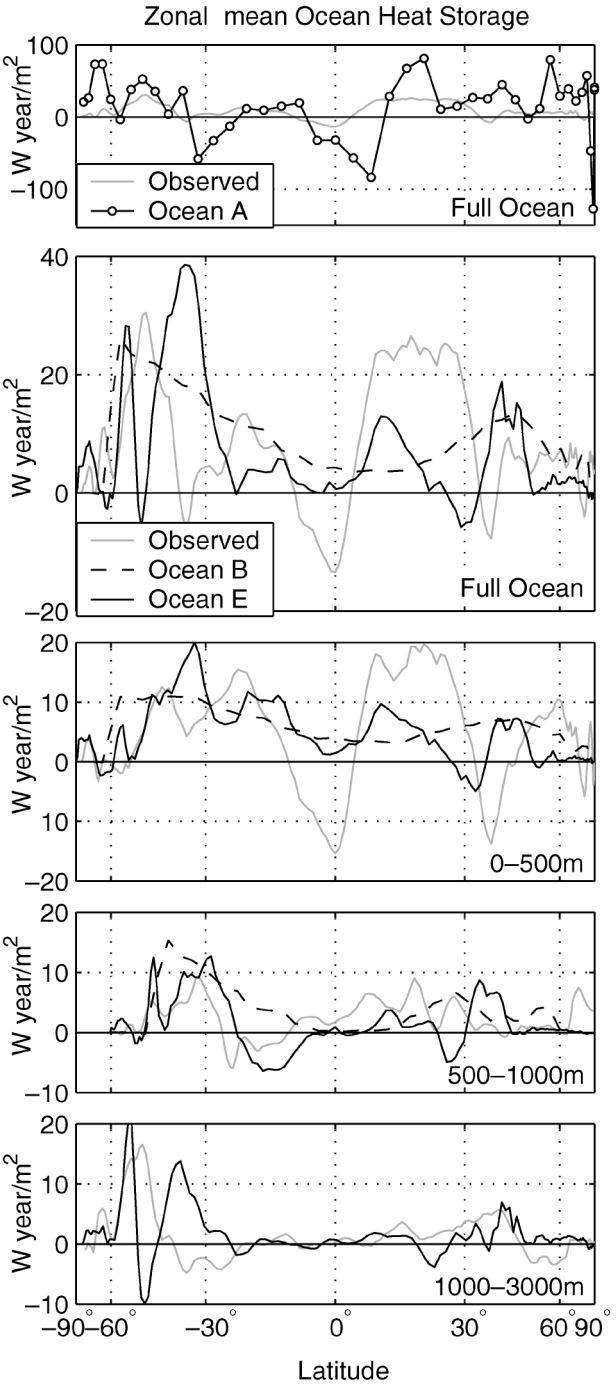

FIG. 5. Zonal ocean heat storage (W yr m^{-2} averaged over the earth's surface) between 1951 and 1998 for (top) the full ocean and successive ocean layers. Observations are from Levitus et al. (2000). Climate models with oceans B and E are forced with five forcings.

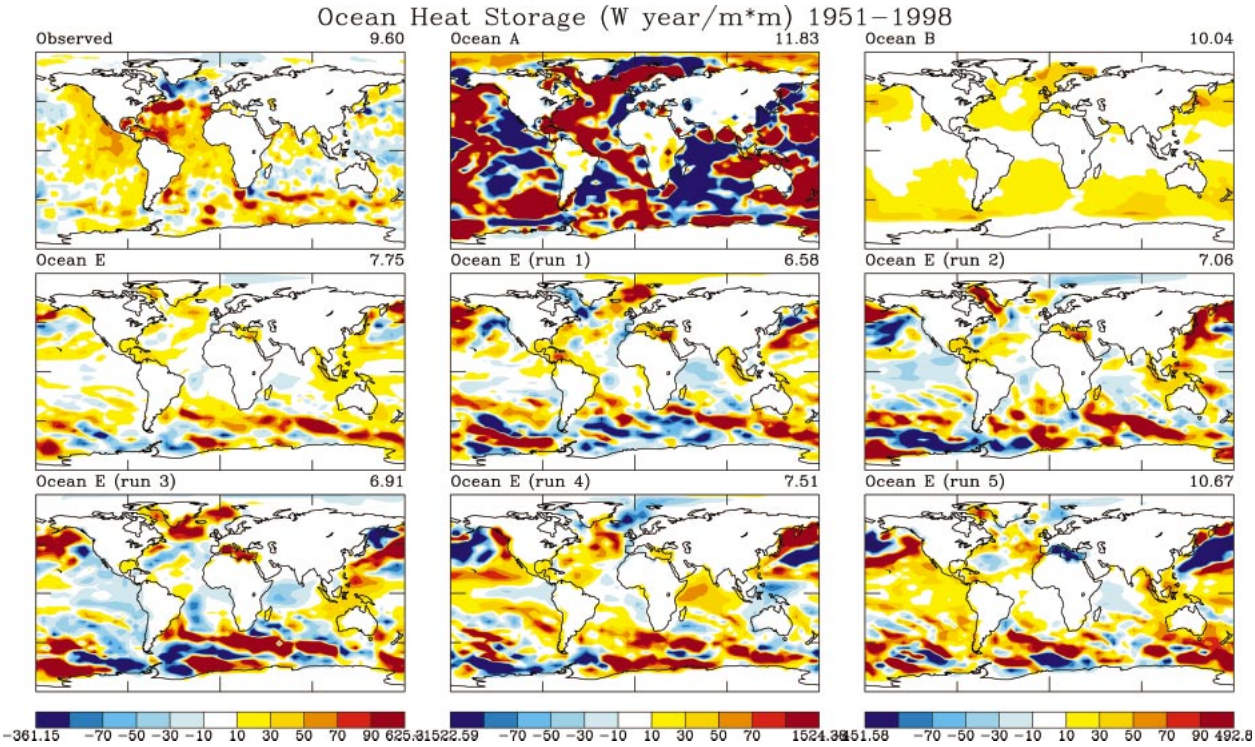

FIG. 6. Global distribution of ocean heat storage during the interval 1951–98. Observations are from Levitus et al. (2000). Climate models with oceans A, B, and E are forced with five forcings.

cooled there in recent decades. In reality, that ocean region may have transmitted extra heat to the atmosphere that helped warm Eurasia in recent decades, but proper modeling of this phenomenon requires simulating anomalies of ocean heat transports and it probably also requires realistic simulation of dynamical interactions with the stratosphere. Note in Fig. 5 that, despite these regions where the sign of the surface heat flux anomaly differs from the change in ocean heat content, ocean A qualitatively captures much of the latitudinal variation of ocean heat storage, which suggests that much of the ocean transport of heat anomalies is zonal. The spikes in heat storage calculated with ocean A in regions of sea ice are a result of changing sea ice area in the dataset of Rayner et al. (2003). The sea ice trends are very uncertain, but the absence of corresponding heat storage spikes in the Levitus et al. data does not rule against the reality of the sea ice changes. A large change in ocean heat storage, as calculated with ocean A, should occur in regions where sea ice cover changes, but within the real ocean the heat content anomaly is likely to be smoothed by ocean transports.

Ocean B yields a distribution of heat storage that is much more featureless than observations, which is not surprising, given the model's lack of dynamical ocean variability. Atmospheric dynamics by itself could produce geographic features in the ocean heat storage, and, for example, one might hope that the Q-flux model would produce the observed negative heat storage in the Baffin Bay region, if the observed trend in the Arctic Oscillation is driven by increasing greenhouse gases (Shindell et al. 2001b). However, the rigid top of the SI2000 model at 10 hPa prevents realistic simulation of that phenomenon in the present simulations with any of oceans A, B, and E.

Oceans B and E both produce a maximum in heat storage in a circum-Antarctic belt, as in observations, with the ocean E results appearing more realistic (Fig. 6). Note the large variability in the heat storage from run to run. Runs 4 and 5 of ocean E have a number of geographic features in common with the observations, including the positive heat content anomalies in the eastern Pacific Ocean. The warm waters off the U.S. West Coast have had biological consequences that have been suggested to be a consequence of global warming (Roemmich and McGowan 1995). The variability among the ensemble members in our simulations for 1951–2000, by itself, would suggest that this warming is a dynamical fluctuation, rather than a forced change, and thus it is as likely as not to revert to cooler temperatures in coming years. However, the simulations below for the next 50 yr present a rather different conclusion.

5. Extended simulations

We extend ensembles of the coupled atmosphere–ocean simulations to 2050 using both the strong (BAU)

and weak (ALT) forcing scenarios. For the sake of interpreting the results we also compare a doubled CO_2 simulation using the HYCOM ocean to a doubled CO_2 run using the Q-flux ocean.

a. Simulations to 2050

Figure 7 shows the ensemble mean transient response of the coupled atmosphere–ocean model with ocean E. During 1951–2000 the climate forcings are the five-forcing and six-forcing scenarios (section 3), so the left side of the figure summarizes results presented in section 4. Two five-member ensembles of runs were extended to 2050 using the BAU and ALT climate forcing scenarios, which, respectively, add forcings of 2.9 and 1.1 W m^{-2} in the 50 yr (section 3). Ocean initial conditions in 2000 were those from the 1951–2000 five-forcing runs. The transient responses to these forcing scenarios are shown in the right half of Fig. 7.

The stratosphere cools almost 1°C in the BAU scenario but only a few tenths of a degree in the ALT scenario, in accord with their increases of CO_2. If the effect of anticipated partial ozone recovery (from chlorine-induced O_3 depletion during the past 25 yr) were included, the stratospheric temperature would be essentially flat during the next 50 yr in the ALT scenario. These results for stratospheric temperature are similar to those obtained with ocean B by Hansen et al. (2002).

The troposphere and surface warm by only 0.3°–0.4°C in the next 50 yr in the ALT scenario, but by more than 1°C in the BAU scenario. These warmings are less than those obtained with ocean B using the same forcing scenarios (Hansen et al. 2002). For example, the warming obtained by Hansen et al. (2002) for the ALT scenario with ocean B is 3/4°C, about twice as large as the warming with ocean E. Consistent with the smaller surface warming with ocean E, the planetary energy imbalance by 2050 increases to ~1.3 W m^{-2} and almost 2 W m^{-2} in the ALT and BAU scenarios, respectively, which compares with 0.8 and 1.4 W m^{-2} for the same scenarios with ocean B (Hansen et al. 2002).

1) HEAT STORAGE

Figures 8 and 9 contrast the ocean heat storage of oceans B and E during the period 2000–50. Both models sequester heat most effectively in high-latitude regions. The prime difference between the two oceans is that ocean E stores more heat at low latitudes, especially in the eastern Pacific Ocean, but also in the western Pacific and Indian Oceans. The greater low-latitude heat storage in ocean E occurs in the upper 500 m (Fig. 9). Table 1 summarizes the observed and modeled global ocean heat storage.

Oceans B and E have similar latitudinal distributions of depth-integrated heat storage (Fig. 9). However, in ocean B a greater amount of heat builds up in the 500–1000-m layer. If an artificial bottom had not been placed at 1 km in ocean B, heat would have penetrated into the lower ocean layers, providing better correspondence with ocean E. This would have 1) increased the mixing of heat from the top ocean layers into the deeper ocean; 2) increased the total ocean heat storage, that is, the heat flux into the ocean surface; and 3) decreased the global surface warming.

The large observed ocean heat storage at low latitudes (Figs. 5 and 6) tends to support the larger magnitude of storage at low latitudes in ocean E, as opposed to ocean B. Larger mixing coefficients may be appropriate at low latitudes, where most of the mixing occurs via quasi-horizontal transports (Ledwell et al. 1998). However, Forest et al. (2002) show that there is a large range of ocean heat uptakes among the different ocean models and, given the uncertainties in observed heat uptake, it seems best to leave Q-flux coefficients as they are. Indeed, Fig. 5 suggests that the Q-flux model does a good job for heat uptake, so the only change needed may be to place the ocean bottom at 4 km.

There are some consistent features in the geographical patterns of simulated heat storage with ocean E that imply predictions for climate change in the coming half-century. Four of the five ensemble members for the ALT scenario and all five of the BAU ensemble members have increased heat storage along the west coast of the Americas. Similarly, both of the forcing scenarios consistently yield a region of decreased heat storage in the Pacific Ocean between about 30° and 60°N. These anomaly patterns have been observed during recent decades and are often suggested to be cyclical. However, our climate simulations suggest that a tendency to have these patterns may be a consequence of the forcings, and thus these ocean temperatures may be a harbinger of climate patterns that will tend to exist in coming decades, rather than being dynamical fluctuations. Cai and Whetton (2001) noted a shift in observed warming from higher latitudes to the El Niño regions, and they presented modeling evidence that the shift was driven by greenhouse gases and was likely to continue.

The large heat storage in both ocean models B and E in the first half of the twenty-first century, despite the very modest increase in climate forcings in the ALT scenario, is a reflection of the current planetary radiation imbalance of 3/4 W m^{-2}, which was inferred several years ago (Hansen et al. 1997) and which is contained in the climate simulations for both ocean models (Fig. 7d). If ocean heat storage is monitored accurately in coming decades it will provide an invaluable diagnostic of the climate system, both for the purpose of refining our knowledge of the planetary energy imbalance, which is important for determining future global climate change, and for the purpose of checking the ocean models' abilities to simulate the distribution of heat anomalies, which is necessary for predicting the geographical distribution of climate change.

2) OCEAN TRANSPORTS

Figure 10 shows the northward heat transport in the ocean basins[3] and globally for ocean E simulations. Results are shown for the past decade with the five-forcings scenario and for 2045–55 with the strongest (BAU) forcing scenario. The simulated heat transports are mostly in agreement with analyses of MacDonald (1998) and Trenberth and Caron (2001), within the margin of observational error. We do not find a noticeable sensitivity of the ocean transport to the climate forcings over the range of forcings that we considered.

We also find no significant impact of the forcings on the ocean E simulated overturning rate and meridional heat flux in the Atlantic Ocean, as shown in Fig. 11. This is consistent with the results of Sun and Bleck (2001), who found that ocean E maintains a stable thermohaline circulation (THC) in a $2 \times CO_2$ experiment that started from observed ocean conditions, but it differs from a number of models that project the thermohaline circulation to weaken in the twenty-first century. Wood et al. (1999) and Dixon et al. (1999) found the thermohaline circulation to slow after 150–200 yr; it also slowed but then recovered by year 500 in the experiment of Manabe and Stouffer (1994). On the other hand, Latif et al. (2000) and Gent (2001) did not find a slowdown of the thermohaline circulation. The wide range of responses of the thermohaline circulation among different climate models is illustrated in Fig. 9.21 of Houghton et al. (2001).

The strength of oceanic overturning is controlled by many factors including the intensity of thermal and haline forcing. Some model studies have shown that increasing surface freshwater fluxes into the North Atlantic are the primary reason for the slowdown of the Atlantic THC in simulations of global warming (Wiebe and Weaver 1999; Dixon et al. 1999), while in other simulations it appears to be the surface warming trend that causes the THC to weaken (Mikolajewicz and Voss 2000). We see in the BAU scenario an increase in both precipitation and evaporation in the North Atlantic in ocean E, which leads to a small overall change in freshwater fluxes. In our experiments, the thermohaline signals, rather than being trapped near the surface, fairly quickly propagate down the water column in the northern North Atlantic. As a result, the vertical stratification in that region remains similar to that in the control run and thus does not impede the sinking motion, which is an essential part of the Atlantic THC. The positive feedback aspects of this process are rather obvious: a strong THC is able to maintain the weak stratification in the sinking region and hence can maintain itself, while a THC that is anemic to begin with may come to a halt during global warming. We note that the Atlantic thermohaline circulation in our simulation (~22 Sv) is strong compared with some recent observational analyses (Ganachaud and Wunsch 2000), but there is a large uncertainty in the observed value.

The range of results among different ocean models is not surprising, as vertical mixing is known to play a major role in long-term, planetary-scale ocean dynamics (Stommel and Arons 1960), and circulation systems driven by buoyancy forces are particularly sensitive to the rate at which buoyancy anomalies are diffused in the ocean. In this vein, Houghton et al. (2001) suggest that differences in subgrid-scale mixing parameterization account for much of the difference in the rate of surface warming. Some vertical mixing is likely to occur as a result of vertical advection whose numerical implementation varies widely among ocean models. Isopycnic coordinate ocean models, due to the quasi-Lagrangian nature of their coordinate surfaces, have an inherent advantage in suppressing the numerical diapycnal mixing associated in the traditional fixed-grid models with the passage of internal waves (Bleck 1998). Gent et al. (2002) also found improvement in modeled meridional overturning circulation with a new parameterization of isopycnal mixing in a *z*-coordinate model, and the strength of the simulated thermohaline circulation with such a parameterization did not slow down in the global warming scenario (Gent 2001).

b. Doubled CO_2 experiment

Interpretation of the transient climate experiments is aided by comparison of equilibrium simulations with oceans B and E using a strong identical forcing. In our doubled CO_2 experiment we add 1% CO_2 yr^{-1} until $2 \times CO_2$ is reached at year 70, when the forcing is 3.9 W m^{-2}, after which time the CO_2 concentration is kept fixed.

Ocean B reaches equilibrium global surface temperature response (2.8°C) by year 400, when the heat flux into the ocean has approached, but not quite reached, zero (Fig. 12). Ocean E, after 300 yr, has a remaining energy imbalance of ~0.7 W m^{-2}. Thus the warming of 2°C at year 300 is the response to ~3.2 W m^{-2} forcing, which implies that the equilibrium sensitivity is ~2.4°C for $2 \times CO_2$. That sensitivity is consistent with the 2.8°C sensitivity of the Q-flux model, because of the different amounts of sea ice in the control runs. The ocean E control run has sea ice covering 2% of the world area, while the sea ice covers 4% of the globe in the ocean B control run. We can judge the impact of the sea ice cover from an alternative version of ocean B used by Hansen et al. (2002). This alternative version had 6% sea ice in the control run, but otherwise identical physics with the Q-flux run used here. The change of sea ice from 4% to 6% of the global area increased the sensitivity from 2.8° to 3.2°C for $2 \times CO_2$.

Other things being equal, a model with 2.4°C sen-

[3] To remove the ambiguity associated with the nonzero meridional mass flux in both the Pacific and Indian Oceans south of the Indonesian passage, the heat flux curves for both basins have been adjusted by the amount of heat transported through that passage.

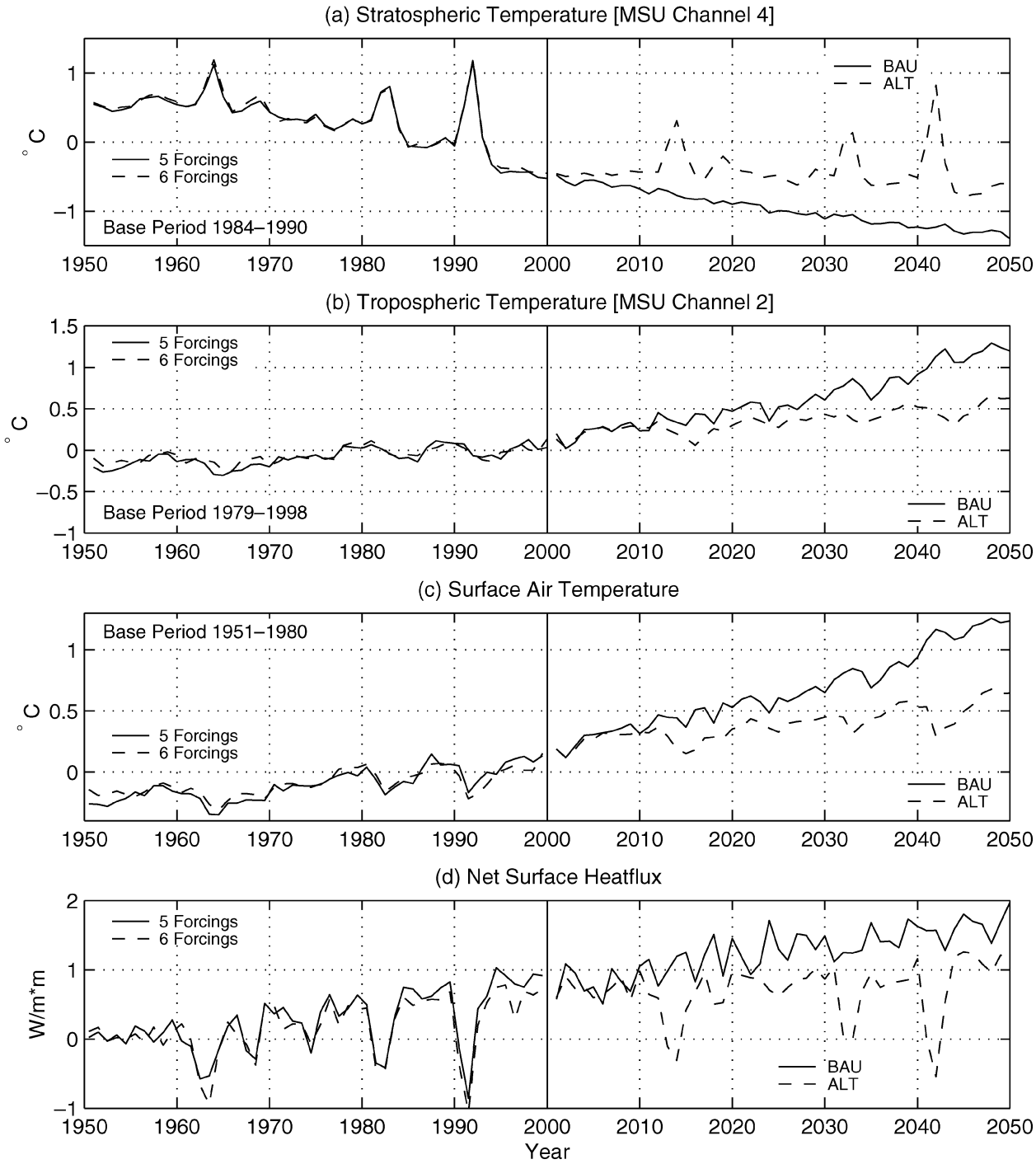

FIG. 7. Ensemble mean transient response of the coupled model with ocean E. During 1951–2000 the climate forcings are the five forcings and six forcings (tropospheric aerosols added) defined in Fig. 1. The extensions to 2050 employ the BAU (2.9 W m^{-2}) and ALT (1.1 W m^{-2}) forcings.

sitivity should approach equilibrium much faster than a model with 2.8°C sensitivity, as the response time is proportional to the square of the equilibrium sensitivity (Hansen et al. 1985). Furthermore, at any given time the heat flux into the ocean is larger in a higher-sensitivity model, other things being equal. Figure 12b shows that other things are not equal in oceans B and E. The flux into the ocean surface in ocean E keeps up with that for ocean B for the first several decades, and after 50 yr it exceeds that for model B. From the results

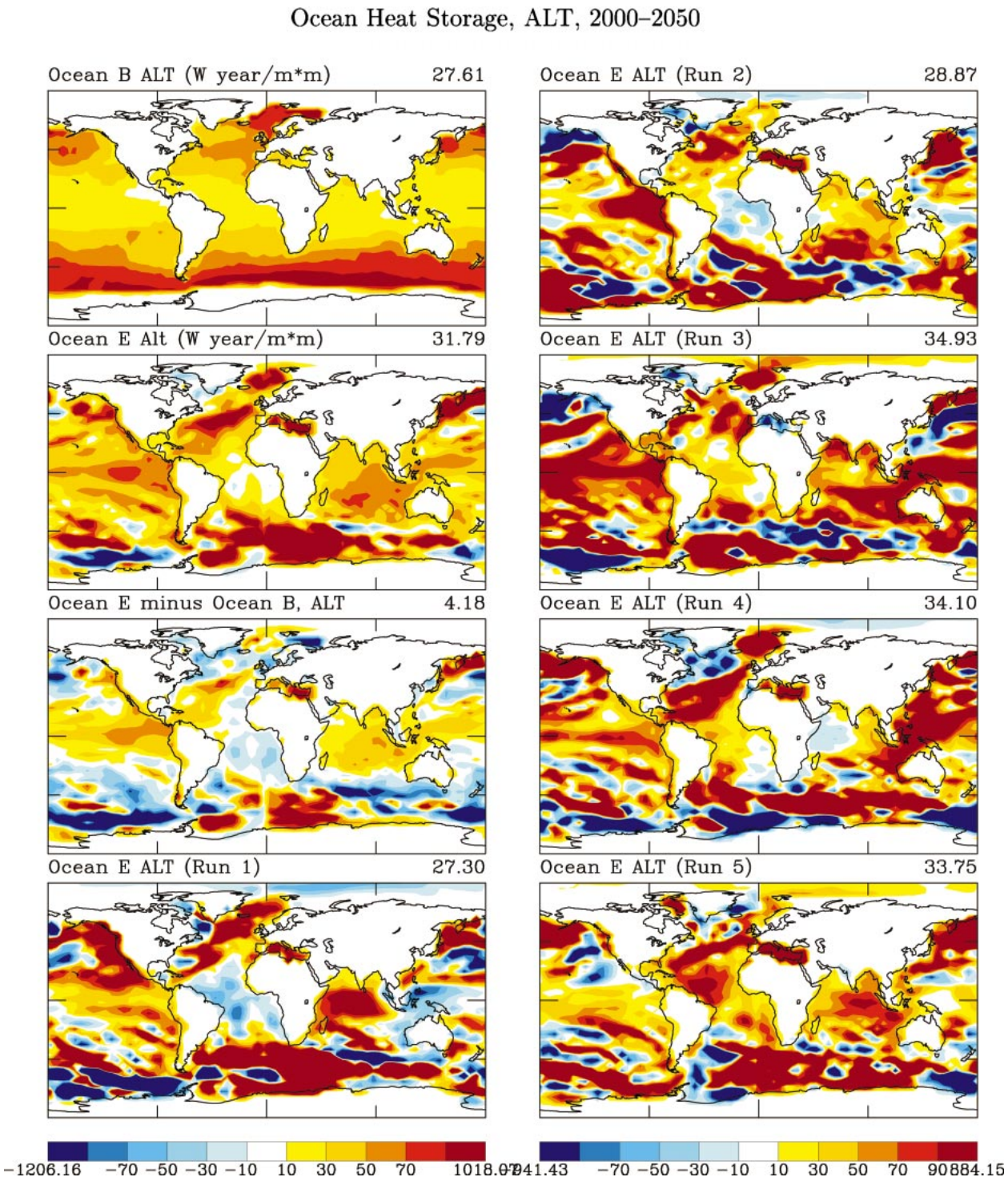

FIG. 8. Ocean heat storage (W yr m^{-2}) during 2000–50 in oceans B and E for the ALT climate forcing scenario.

in section 5.1, we know there are two reasons for this: 1) the shallowness of ocean B model (1 km), and 2) the different vertical diffusions in two oceans, especially the more rapid heat uptake at low latitudes in ocean E. Figure 12b shows that these effects are sufficient to make the heat storage of the model with lower sensitivity (i.e., ocean E) slightly exceed that of ocean B on the 100-yr timescale. This result is consistent with the greater heat storage in ocean E in the transient climate experiment during the period 2000–50 (Table 1).

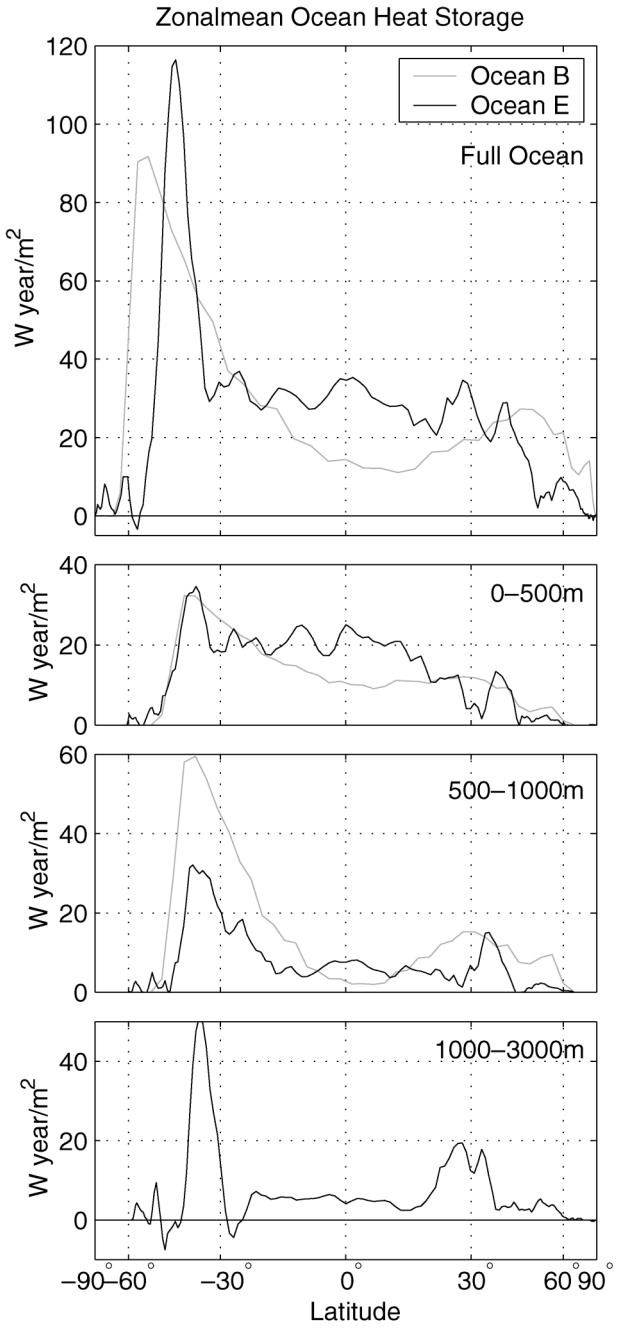

FIG. 9. Zonal ocean heat storage (W yr m^{-2} averaged over the earth's surface) during 2000–50 in oceans B and E for the ALT climate forcing scenario.

6. Discussion

We aim to learn something about the effect of the ocean representation on ocean heat uptake and climate response time by contrasting results from experiments that use a variety of oceans driven by the same atmosphere and climate forcings. Conclusions from the present simulations, for oceans A, B, and E, are constrained by the brevity of the simulations and limitation to a single dynamical ocean model. Some of the computations are necessarily different for these three ocean representations, so we clarify that here.

a. Ocean A

1) GLOBAL OCEAN HEAT STORAGE

The climate model with ocean A is nearly in radiation balance at the beginning of the simulation, that is, in 1951. This near balance occurs because the parameter in the model that controls cloud cover (Uoo, the minimum grid-box mean humidity at which clouds begin to form) was chosen with the objective of radiation balance. However, even a small planetary radiation imbalance needs to be evaluated, because it affects the ocean heat storage. We can determine the radiation imbalance in the climate model by making a long run with fixed 1951 SST and atmospheric composition. However, it is better to use the mean SST for several years centered on 1951 to minimize the effect of interannual SST variability, such as El Niño.

Specifically, Hansen et al. (2002) made a 20-yr simulation with 1951 atmospheric composition and with SST and sea ice based on the 10-yr mean of Rayner et al. (2003) centered on 1 January 1951, obtaining a flux imbalance of -0.175 W m^{-2}. In other words, in the control run the planet continually gives out heat to space at an annually averaged rate of 0.175 W m^{-2}, as the fixed ocean temperature does not respond to the energy loss. The standard deviation of the annual mean global radiation balance was 0.18 W m^{-2}, so, for the assumed SST distribution, the uncertainty in the calculated flux imbalance is of order 0.04 W m^{-2}. Thus, if we wish to assume that the planet was in energy balance in the 1951 era and use the energy imbalance in the transient 1951–98 ocean A simulations to calculate ocean heat storage, we must add 0.175 W m^{-2} to the calculated fluxes.

The resulting ocean heat storage in ocean A is shown by the green curve in Fig. 13, for the case of the six climate forcings of Fig. 1. The heat storage between 1951 and 1998 is $\sim$3 W yr m^{-2}, which is much less than the observed heat storage of $\sim$10 W yr m^{-2}. We could achieve greater heat storage by increasing the growth of the net climate forcing over the period 1951–98. For example, if there were an unknown climate forcing that increased linearly by 0.2 W m^{-2} over the 47-yr period it would add to the heat storage 4.7 W m^{-2}. Thus a forcing that increased by 0.3–0.4 W m^{-2} over the 47-yr period would be sufficient to yield agreement with the observed ocean heat storage. Such an error in our net climate forcing cannot be ruled out.

However, we believe that a more likely interpretation is that the planet was not in energy balance in 1951. The red curve in Fig. 13 shows that an energy imbalance of $\sim$0.18 W m^{-2} (energy coming into the planet) is needed for approximate agreement with observed ocean heat storage. Because of the uncertainty in the climate

TABLE 1. Ocean heat storage (W yr m^{-2}) in observations (Levitus et al. 2000) and in ocean models B and E. The models are driven by five forcings during 1951–98 and by the ALT forcing scenario during 2000–50.

	1951–98			2000-50	
Ocean depth	Observed	Ocean B	Ocean E	Ocean B	Ocean E
0–500 m	5.0	6.0	5.6	13.2	17.0
500–1000 m	2.3	4.0	1.2	14.4	8.2
1000–1500 m	0.7	—	0.7	—	3.9
1500–2000 m	0.4	—	0.6	—	1.8
2000–2500 m	0.2	—	0.4	—	1.4
2500–3000 m	0.0	—	0.3	—	0.6
Full ocean	8.6	10.0	8.1	27.6	30.8

forcing, this inferred energy imbalance is uncertain by an amount comparable to the estimated imbalance. All we can say is that, for our best estimate of climate forcing, we require a planetary energy imbalance of $+0.18$ W m^{-2} in 1951 to obtain the ocean heat storage measured by Levitus et al. (2001). An energy imbalance of 0.18 W m^{-2} in 1951 can be compared with the imbalance of 0.65 W m^{-2} in 1979 inferred by Hansen et al. (1997) and the imbalance of 3/4 W m^{-2} in 1998 inferred by Hansen et al. (2002) and by our present simulations. These values are consistent, as only ~30% of the present greenhouse gas climate forcing was introduced prior to 1951 and the earlier forcing was added over a longer period.

2) TEMPORAL AND GEOGRAPHICAL VARIATIONS

The calculated global heat storage with ocean A as a function of time (Fig. 2d) does not yield the strong decadal fluctuations in the Levitus et al. (2000) data, such as the rapid decrease in the mid-1950s, increase in the early 1970s, and decrease in the early 1980s. Although fluctuations in ocean dynamics can cause fluctuations in ocean heat content unrelated to climate forcings, the ocean heat content fluctuations must be accompanied by a flux anomaly across the ocean surface. However, when we use observed SST to calculate the fluxes, we do not find anomalies corresponding to these supposed rapid ocean heat content changes. Therefore, we suggest that the ocean A calculations cast doubt on the reality of these decadal fluctuations in ocean heat content. Alternatively, our climate model may not produce correct flux anomalies as a function of SST. For example, there may have been real-world flux anomalies associated with wind anomalies or cloud cover anomalies that are not captured by our model. A third possibility is error in the specified sea ice history, because sea ice changes strongly influence ocean–atmosphere heat exchange. Analysis of the regional distribution of the heat content fluctuations may discriminate among alternative interpretations.

The local heat storage anomalies calculated with ocean A account only for the simulated exchange of heat at the ocean surface. Thus comparison of the ocean A result with observed ocean heat content yields inferences about ocean dynamical heat transports. For example, the surface heat fluxes in ocean A (Fig. 6) have the eastern Pacific Ocean (a region with good observations) disgorging heat at a substantial rate in just the region where the Levitus et al. (2000) analyses show that the ocean heat content also increased markedly. This implies that there was a substantial horizontal transport of heat by the ocean into this region.

b. Ocean B

The SST response to climate forcings is larger for ocean B than for ocean E. We have identified three

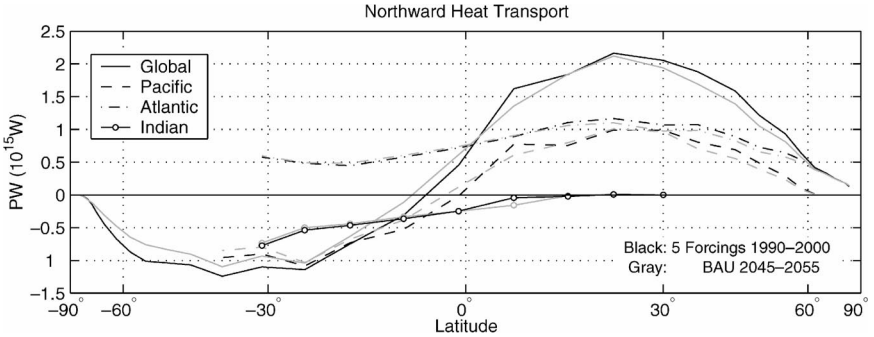

FIG. 10. Northward heat transport in three ocean basins and globally in ocean E simulations for the past decade and simulations for the middle of the twenty-first century with a strong (BAU) forcing scenario.

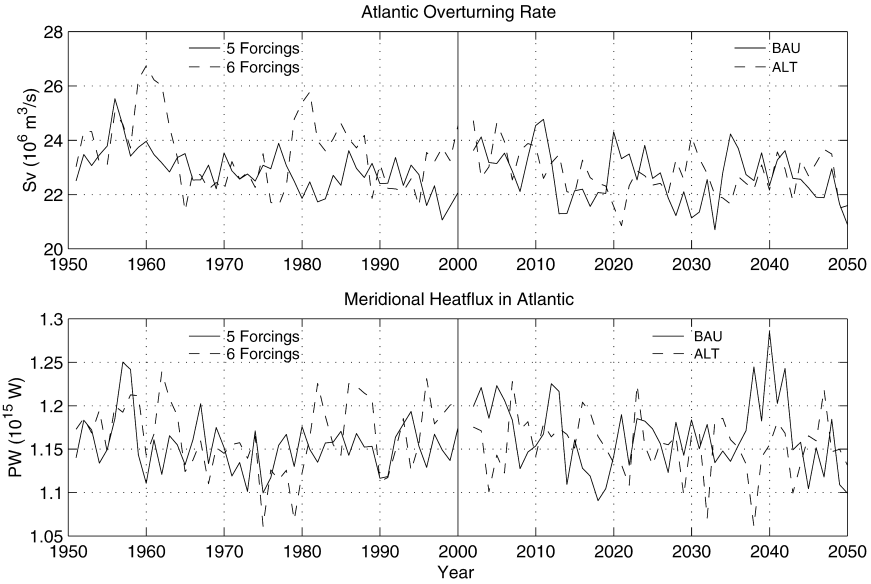

FIG. 11. Overturning rate (Sv) and meridional heat transport (PW) in the Atlantic Ocean in simulations with ocean E for the same forcing scenarios as in Fig. 7.

reasons that contribute to this. The first is the ocean floor at 1-km depth in ocean B, which prevents heat diffusion to greater depth and thus increases surface warming. This flaw was included in the Q-flux model at its inception (Hansen et al. 1984) for the sake of computational convenience. It should have no detectable effect on short simulations such as those for the satellite era (Hansen et al. 1997). However, in simulations that begin in 1951 the heat storage at 500–1000 m by 1998 is already of a magnitude comparable to that at 0–500 m (Fig. 5), so we suspect that surface warming by 2050 is significantly increased by the artificial ocean bottom at 1 km.

The second reason for the larger SST response with ocean B is the lesser heat storage in the Tropics during 2000–50, compared with ocean E. Here too, we suspect that ocean B is more likely to be at fault. The basis for this suspicion is the large observed heat storage at low latitudes in the past 50 yr (Figs. 5 and 6). By itself, this empirical evidence is not convincing, though, as heat gains in recent decades could be associated with a natural fluctuation, such as a change of the intensity of ENSOs, rather than being driven by the trend in global climate forcings. However, ocean E is expected to yield realistic quasi-horizontal heat transfer and thus it may be more capable than ocean B in simulating the sequestering of heat in the ocean at low latitudes.

The third reason for a larger response with ocean B than with ocean E is its greater equilibrium climate sensitivity, their sensitivities to doubled CO_2 being 2.8° and ~2.4°C, respectively. In this case, the evidence is more in favor of ocean B than ocean E. Empirical evidence from paleoclimate data suggests a climate sensitivity of 3° ± 1°C for 2 × CO_2. Although this is consistent with either 2.4° or 2.8°C, it favors the latter. Moreover, the smaller sensitivity with ocean E is likely to be due to the smaller amount of sea ice in its control run, which is only about half of present-day sea ice amount.

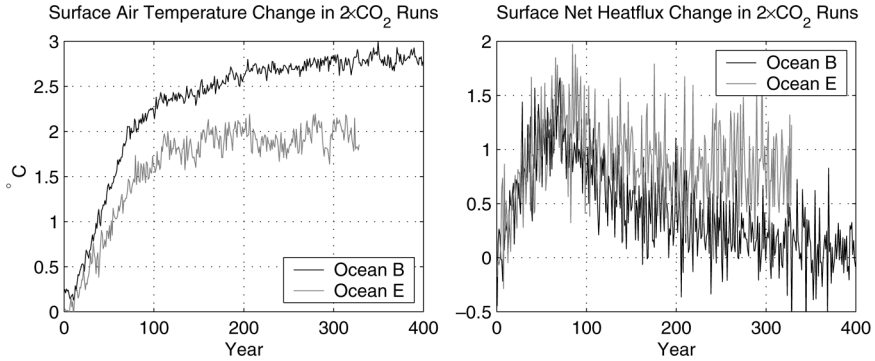

FIG. 12. Changes of surface air temperature and net heat flux into the ocean in 2 × CO_2 experiment.

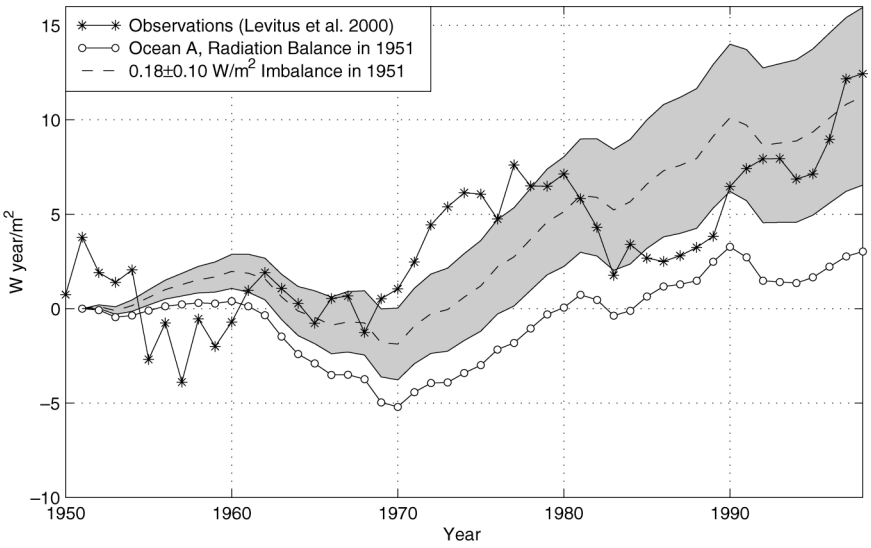

FIG. 13. Ocean heat content anomaly (W yr m^{-2}) averaged over the surface of the earth. Zero point for model is 1951. Zero point for observations is 1950–59 mean.

Larger uptake of heat in ocean E than in ocean B is not surprising. Diffusion in ocean B, based on empirical fit to transient tracer data and meant to represent the effect of all mixing processes, varies from about 0.1 $cm^2\ s^{-1}$ at low latitudes to 15 $cm^2\ s^{-1}$ in the North Atlantic Ocean and in the Southern Ocean (Hansen et al. 1984). Prescribed diapycnal diffusion in ocean E (0.003 $cm^2\ s^{-2} \times N^{-1}$) is generally smaller than the total diffusion in ocean B, but the net effect of all mixing processes in ocean E yields a greater effective diffusion, at the high end of the range of ocean models examined by Sokolov et al. (2003), as discussed below. Analysis of the ocean heat uptake processes is beyond the scope of the present paper, but we anticipate that new longer simulations that correct several flaws in the present runs, include other dynamical ocean models, and test alternative turbulent mixing schemes, will provide fodder for useful analyses.

Overall, comparison of the ocean B heat storage with observations and with ocean E provides a positive assessment of ocean B capabilities. The too-shallow bottom is trivial to correct and the tropical mixing rates could be modified if more well-founded values were defined. The Q-flux model perhaps has been unjustly denigrated in the past, for example, not being considered as a coupled atmosphere–ocean model and excluded from Houghton et al. (1996) comparisons, despite other limitations of many dynamical oceans, such as flux corrections and the absence of polar coverage. However, we consider ocean B's principal value not as a competitor to dynamic ocean models, but rather as a companion that helps to improve our understanding of the mechanisms and significance of results from more realistic ocean models.

c. Ocean E

The heat sequestration in ocean E has a good deal in common with observed heat storage in the past half century. The profiles of heat storage versus depth (Fig. 4) and versus latitude (Fig. 5) are generally consistent with the observational analysis of Levitus et al. (2000). Geographic patterns of simulated heat storage (Fig. 6) are not quite as faithful to observations. The positive heat storage in the circum-Antarctic belt and heat loss in the North Pacific Ocean are captured by all runs of the model, and some of the individual runs capture the positive heat storage off the west coast of North America and in the North Atlantic Ocean. Overall, the simulated heat storage is sufficiently realistic that it perhaps adds to the credibility of the model already documented by Sun and Bleck (2001), and it suggests that it would be interesting to carry out global and regional climate studies using this ocean model combined with an atmospheric model capable of representing the primary climate forcings including those operating via the stratosphere.

d. Reconciliation of oceans A, B, and E

Ocean A provides evidence that the earth was out of radiation balance in 1951 by, we estimate, $\sim$0.2 W m^{-2}. In lieu of starting climate simulations at an earlier date, climate models initiated in 1951 could include a positive radiative input of that magnitude. This is not a perfect solution to the cold start problem, as it does not provide a temperature anomaly profile within the ocean, but it should be a useful approximation.

If our ocean E simulations had included this ''initial imbalance'' forcing, global warming by 2000 probably

would have increased ~0.1°C (more than half of the equilibrium response should be achieved in 50 yr) bringing the result into closer agreement with observations (Fig. 2). Increased climate sensitivity of the model (if it had 4% sea ice instead of 2%) should add a few hundredths of a degree to the response over 50 yr. Given uncertainties in the climate forcings and observed temperature change, as well as unforced variability of climate, the correspondence with observed global temperature change is excellent.

If the same initial planetary energy imbalance had been included in the ocean B simulations of Hansen et al. (2002), it would have increased global warming 0.1°C, making the simulated warming somewhat larger than observed. However, the other factors discussed above, the need to extend the ocean depth to 4 km and perhaps increase the mixing rate in the Tropics, would reduce the surface warming. The net change from all these refinements is probably small.

7. Implications

a. Projected climate change

Based on results from the different ocean models, we estimate that the global warming in the next 50 yr with the alternative scenario of climate forcings (1.1 W m^{-2} added forcing between 2000 and 2050) will be only ~0.5° ± 0.2°C. The partly subjective error estimate assumes that the forcing is precise and thus the error incorporates uncertainties in the atmosphere and ocean representations including climate sensitivity. The warming is less than the 0.75° ± 0.25°C obtained with ocean B (Hansen et al. 2002), because the version of ocean B used in that study is at least somewhat deficient in its ability to sequester heat. The warming is greater than the 0.3°–0.4°C in our current ocean E simulation because of the deficient sea ice in ocean E (and thus low climate sensitivity) and the remaining effect in 2000–50 of the 1951 cold start of that model.

We stress that we are not predicting attainment of the alternative scenario of climate forcings, although we think such a scenario is achievable. It is an ambitious scenario for slowing the growth rate of climate forcings that would require non-CO_2 forcings to be no greater in 2050 than they are today (Hansen et al. 2002). The growth rate of atmospheric CO_2 in this scenario is only slightly larger in the next two decades than it was in the 1990s and it then begins to decline slowly. The net forcing is less than in any Houghton et al. (2001) scenario.

Increased sequestering of heat by the ocean not only reduces surface warming in coming decades, it also increases the predicted planetary disequilibrium, that is, the earth's energy imbalance. Even with the moderate climate forcing of the alternative scenario and a low climate sensitivity of 2.4°C for 2 × CO_2, the net flux of energy into the planet increases to ~1.3 W m^{-2} in 2050, considerably larger than the 0.75 W m^{-2} estimated for the earth's current imbalance. The fact that more of the greenhouse heating is sequestered and less appears as near-term warming is a consequence of the deep mixing and long response time of the presumably more realistic ocean representation of ocean E. This longer ocean response time has both good and bad sides from a practical perspective. It provides an opportunity to quantitatively verify the track that the earth's climate is on, provided appropriate observations are obtained, and a longer period to act before the largest consequences of global warming will occur. The bad side of the slower response is an increase in the amount of warming that is ''in the pipeline'' but not yet realized. However, this slower response also means that, if the emissions of CO_2 are reduced, the ocean has a longer time to take up CO_2 and thus avoid the largest climate change.

The importance of oceanic sequestering of heat and the implications for climate response time raise the question of how reliable the ocean E result is. Sokolov et al. (2003) compare 11 atmosphere–ocean GCMs and find that their measure of oceanic heat uptake, $K_\nu^{1/2}$, where $K_\nu^{1/2}$ is an effective global diffusion coefficient, varies from 2 to 5 cm $s^{-1/2}$ among models, with ocean E at the large end of this range. Empirical data analyzed by Forest et al. (2002) tend to favor the higher K_ν values, but all of the models are within the range of observational uncertainty. The Levitus et al. (2000) data for heat uptake seem consistent with our ocean E simulation, but do not verify the rate of heat uptake. Although we believe that the ocean E results are realistic, the rate of ocean uptake is uncertain and deserves high priority in modeling and observational analyses.

b. Needed observations

This study highlights the importance of full-ocean heat storage measurements. The current rate of change of ocean heat content provides a measure of the ''residual'' global climate forcing, that is, the existing integrated (net) forcing of the global climate system. We define the residual forcing as that portion of long-term climate forcings that has not yet been responded to. The residual forcing is equal to the current planetary energy imbalance excluding transitory effects such as El Niños and volcanos. Multiplied by global climate sensitivity, estimated to be 3/4° ± 1/4°C (W m^{-2})$^{-1}$, the residual forcing yields the additional global warming that is in the pipeline, that is, the warming that will occur without any further change of atmospheric composition.

The increased heat content of ~7 W yr m^{-2} in the 1990s in the Levitus et al. (2000) data is nominally consistent with our estimated current planetary energy imbalance of 0.75 W m^{-2}, but it is somewhat larger than the heat storage in our simulations, which is reduced by the effect of the Pinatubo eruption. The ocean heat gain over the past half-century is in good agreement with the mean planetary energy imbalance in our climate

model simulations. However, there are decadal variations in the Levitus et al. (2000) data that are not associated with known climate forcings and are not reproduced with any of the ocean models. It is desirable to have more complete ocean measurements, with better geographic and depth sampling, because the existing network could misinterpret a dynamical redistribution of heat as a change of ocean heat content.

The full-ocean depth needs to be monitored. The international Argo project (Roemmich and Owens 2000) will deploy about 3000 profiling floats that will measure temperature to a depth of 1500–2000 m every 10 days on a near-global basis. Although this will be helpful, it must be supplemented by deep-ocean measurements. Because the deeper ocean changes more slowly, the frequency of surveying the deep ocean does not need to be as great as for the upper ocean.

Climate forcing agents must be monitored so that we can understand the causes of changes in ocean heat content. Knowledge of the principal individual forcing agents is also information that decision makers would require, should they wish to alter the course of climate change. Most greenhouse gases, except tropospheric ozone, are well measured, but a large improvement in the quality of measurements of aerosols and their effects on clouds is needed if we are to quantify their changing forcing. There are plans for measurements of aerosols and cloud particles from operational satellites in about 2010 with sufficient information on the microphysics to infer composition specific information (Haas et al. 2002), as well as plans for measuring tropospheric ozone. Thus if ocean heat content measurements are improved, it may be possible to begin to quantify much better the changing planetary radiation imbalance and its causes within about a decade.

c. Future simulations

This study provides an indication of the potential merit of climate simulations in which identical forcings are used to drive climate models with alternative treatments of key parts of the climate system. Although we considered here only three alternative ocean representations, our intention, as discussed by Hansen et al. (1997, 2002), is to include other dynamic ocean models, more realistic stratospheric representations, and models with lower and higher climate sensitivity (via altered cloud feedbacks). This approach differs from comparison of models of different laboratories, because the latter involve uncountable differences among the model physical representations, which thus makes it difficult to identify the causes of different simulated climate responses. The simulations will be more useful if they begin early enough to avoid the cold start problem and if the atmosphere realistically represents troposphere–stratosphere interactions.

Acknowledgments. We are indebted to Rainer Bleck, the architect of the HYCOM model, for his guidance and suggestions; and Wil Burns, Peter Gleick, Peter Stone, and two anonymous referees for reference material and suggestions for the manuscript. This research was supported by the NASA climate and oceanography programs managed by Tsengdar Lee and Eric Lindstrom.

REFERENCES

Arfken, G., 1970: *Mathematical Methods for Physicists.* 2d ed. Academic Press, 815 pp.

Barnett, T. P., D. W. Pierce, and R. Schnur, 2001: Detection of anthropogenic climate change in the world's oceans. *Science,* **292,** 270–274.

Bleck, R., 1998: Ocean modeling in isopycnic coordinates. *Ocean Modeling and Parameterization,* E. P. Chassignet and J. Verron, Eds., Kluwer Academic, 423–448.

——, 2002: An oceanic general circulation model framed in hybrid isopycnic–Cartesian coordinates. *Ocean Model.,* **4,** 55–88.

——, and S. G. Benjamin, 1993: Regional weather prediction with a model combining terrain-following and isentropic coordinates. Part I: Model description. *Mon. Wea. Rev.,* **121,** 1770–1785.

——, C. Rooth, D. Hu, and L. Smith, 1992: Salinity-driven thermocline transients in a wind- and thermohaline-forced isopycnic coordinate model of the North Atlantic. *J. Phys. Oceanogr.,* **22,** 1486–1505.

Boyle, J. S., 1998: Evaluation of the annual cycle of precipitation over the United States in GCMs: AMIP simulations. *J. Climate,* **11,** 1041–1055.

Cai, W., and P. H. Whetton, 2001: A time-varying greenhouse warming pattern and the tropical–extratropical circulation linkage in the Pacific Ocean. *J. Climate,* **14,** 3337–3355.

Christy, J. R., R. W. Spencer, and W. D. Braswell, 2000: MSU tropospheric temperatures: Dataset construction and radiosonde comparisons. *J. Atmos. Oceanic Technol.,* **17,** 1153–1170.

Cubasch, U., K. Hasselmann, H. Hock, E. Maier-Reimer, U. Mikolajewicz, B. D. Santer, and R. Sausen, 1992: Time-dependent greenhouse warming computations with a coupled ocean–atmosphere model. *Climate Dyn.,* **8,** 55–69.

Dixon, K. W., and J. R. Lanzante, 1999: Global mean surface air temperature and North Atlantic overturning in a suite of coupled GCM climate change experiments. *Geophys. Res. Lett.,* **26,** 1885–1888.

——, T. L. Delworth, M. J. Spelman, and R. J. Stouffer, 1999: The influence of transient surface fluxes on North Atlantic overturning in a coupled GCM climate change experiment. *Geophys. Res. Lett.,* **26,** 2749–2752.

Forest, C. E., P. H. Stone, A. P. Sokolov, M. R. Allen, and M. D. Webster, 2002: Quantifying uncertainties in climate system properties with the use of recent climate observations. *Science,* **295,** 113–117.

Ganachaud, A., and C. Wunsch, 2000: Improved estimates of global ocean circulation, heat transport and mixing from hydrographic data. *Nature,* **408,** 453–456.

Gent, P., 2001: Will the North Atlantic Ocean thermohaline circulation weaken during the 21st century? *Geophys. Res. Lett.,* **28,** 1023–1026.

——, A. P. Craig, C. M. Bitz, and J. W. Weatherly, 2002: Parameterization improvements in an eddy-permitting ocean model for climate. *J. Climate,* **15,** 1447–1459.

Haas, J. M., H. Swenson, and S. A. Cota, cited 2002: Aerosol Polarimetry Sensor (APS): A new operational environmental sensor for NPOESS. [Available online at http://npoesslib.ipo.noaa.gov/Released_papers/Aerosol_Polarimetry_Sensor_talk.doc]

Hansen, J., 2000: The Sun's role in long-term climate change. *Space Sci. Rev.,* **94,** 349–356.

——, A. Lacis, D. Rind, G. Russell, P. Stone, I. Fung, R. Ruedy, and J. Lerner, 1984: Climate sensitivity: Analysis of feedback mechanisms. *Climate Processes and Climate Sensitivity, Geophys. Monogr.,* No. 29, Amer. Geophys. Union, 130–163.

——, G. Russell, A. Lacis, I. Fung, D. Rind, and P. Stone, 1985: Climate response times: Dependence on climate sensitivity and ocean mixing. *Science,* **229,** 857–859.

——, I. Fung, A. Lacis, D. Rind, S. Lebedeff, R. Ruedy, G. Russell, and P. Stone, 1988: Global climate changes as forecast by Goddard Institute for Space Studies: Three-dimensional model. *J. Geophys. Res.,* **93,** 9341–9364.

——, A. Lacis, R. Ruedy, M. Sato, and H. Wilson, 1993: How sensitive is the world's climate? *Nat. Geogr. Res. Explor.,* **9,** 142–158.

——, and Coauthors, 1997: Forcings and chaos in interannual to decadal climate change. *J. Geophys. Res.,* **102,** 25 679–25 720.

——, R. Ruedy, M. Sato, M. Imhoff, W. Lawrence, D. Easterling, T. Peterson, and T. Karl, 2001: A closer look at United States and global surface air temperature change. *J. Geophys. Res.,* **106,** 23 947–23 963.

——, and Coauthors, 2002: Climate forcings in Goddard Institute for Space Studies SI2000 simulations. *J. Geophys. Res.,* **107** (D18), 4347, doi:10.1029/2001JD001143.

Houghton, J. T., L. G. Meira Filho, B. A. Callander, N. Harris, A. Kattenberg, and K. Maskell, Eds.,1996: *Climate Change 1995: The Science of Climate Change.* Cambridge University Press, 572 pp.

——, Y. Ding, D. J. Griggs, M. Nouger, P. J. van der Linden, and D. Xiaosu, Eds.,2001: *Climate Change 2001: The Scientific Basis.* Cambridge University Press, 881 pp.

Huang, B., P. H. Stone, A. P. Sokolov, and I. V. Kamenkovich, 2003: The deep-ocean heat updake in transient climate change. *J. Climate,* **16,** 1352–1363.

Jones, P. D., M. New, D. E. Parker, S. Martin, and I. G. Rigor, 1999: Surface air temperature and its changes over the past 150 years. *Rev. Geophys.,* **37,** 173–199.

Lamb, H. H., 1977: *Climate: Present, Past and Future.* Methuen, 835 pp.

Latif, M., E. Roeckner, U. Mikolajewicz, and R. Voss, 2000: Tropical stabilization of the thermohaline circulation in a greenhouse warming simulation. *J. Climate,* **13,** 1809–1813.

Ledwell, J. R., A. J. Watson, and C. S. Low, 1998: Mixing of a tracer in the pycnocline. *J. Geophys. Res.,* **103,** 21 499–21 529.

Levitus, S., and T. P. Boyer, 1994: *Temperature*. Vol. 4, *World Ocean Atlas 1994,* NOAA Atlas NESOIS 4, 117 pp.

——, R. Burgett, and T. P. Boyer, 1994: *Salinity*. Vol. 3, *World Ocean Atlas 1994,* NOAA Atlas NESDIS 3, 99 pp.

——, J. I. Antonov, T. P. Boyer, and C. Stephens, 2000: Warming of the world ocean. *Science,* **287,** 2225–2229.

——, ——, J. Wang, T. L. Delworth, K. W. Dixon, and A. J. Broccoli, 2001: Anthropogenic warming of Earth's climate system. *Science,* **292,** 267–270.

MacDonald, A. M., 1998: The global ocean circulation: A hydrographic estimate and regional analysis. *Progress in Oceanography,* Vol. 41, Pergamon, 281–382.

Manabe, S., and R. J. Stouffer, 1994: Multiple-century response of a coupled ocean–atmosphere model to an increase of atmospheric carbon dioxide. *J. Climate,* **7,** 5–23.

——, ——, M. J. Spelman, and K. Bryan, 1991: Transient responses of a coupled ocean–atmosphere model to gradual changes of CO_2. Part I: Annual mean response. *J. Climate,* **4,** 785–818.

Mann, M. E., R. S. Bradley, and M. K. Hughes, 1998: Global-scale temperature patterns and climate forcing over the past six centuries. *Nature,* **392,** 779–787.

Meehl, G. A., W. M. Washington, and T. R. Karl, 1993: Low frequency variability and CO_2 transient climate change. Part I: Time-averaged differences. *Climate Dyn.,* **8,** 117–133.

Mikolajewicz, U., and R. Voss, 2000: The role of the individual air–sea flux components in CO_2-induced changes of the ocean's circulation and climate. *Climate Dyn.,* **16,** 627–642.

Mitchell, J. F. B., T. C. Johns, J. M. Gregory, and S. F. B. Tett, 1995: Climate response to increasing levels of greenhouse gases and sulphate aerosols. *Nature,* **376,** 501–504.

Neelin, J. D., and H. A. Dijkstra, 1995: Ocean–atmosphere interaction and the tropical climatology. Part I: The dangers of flux adjustment. *J. Climate,* **8,** 1325–1342.

Parker, D. E., M. Gordon, D. P. N. Cullum, D. M. H. Sexton, C. K. Folland, and N. Rayner, 1997: A new global gridded radiosonde temperature data base and recent temperature trends. *Geophys. Res. Lett.,* **24,** 1499–1502.

Prather, M. J., 1986: Numerical advection by conservation of second-order moments. *J. Geophys. Res.,* **91,** 6671–6680.

Rayner, N., D. E. Parker, C. K. Folland, E. B. Horton, L. V. Alexander, and D. P. Rowell, 2003: The global sea-ice and sea surface temperature (HadISST) data sets. *J. Geophys. Res.,* in press.

Roemmich, D., and J. McGowan, 1995: Climatic warming and the decline of zooplankton in the California Current. *Science,* **267,** 1324–1326.

——, and W. B. Owens, 2000: The Argo project: Global ocean observations for understanding and prediction of climate variability. *Oceanography,* **13,** 45–50.

Russell, G. L., and J. A. Lerner, 1981: A new finite-differencing scheme for the tracer transport equation. *J. Appl. Meteor.,* **20,** 1483–1498.

——, J. R. Miller, D. Rind, R. Ruedy, G. Schmidt, and S. Sheth, 2000: Comparison of model and observed regional temperature changes during the past 40 years. *J. Geophys. Res.,* **105,** 14 891–14 898.

Santer, B. D., T. M. L. Wigley, J. S. Boyle, D. J. Gaffen, J. J. Hnilo, D. Nychka, D. E. Parker, and K. E. Taylor, 2000: Statistical significance of trends and trend differences in layer-average atmospheric temperature time series. *J. Geophys. Res.,* **105,** 7337–7356.

Shindell, D. T., G. A. Schmidt, M. E. Mann, D. Rind, and A. Waple, 2001a: Solar forcing of regional climate change during the Maunder Minimum. *Science,* **294,** 2149–2152.

——, ——, R. L. Miller, and D. Rind, 2001b: Northern Hemisphere winter climate response to greenhouse gas, ozone, solar, and volcanic forcing. *J. Geophys. Res.,* **106,** 7193–7210.

Sokolov, A. P., C. E. Forest, and P. H. Stone, 2003: Comparing oceanic heat uptake in AOGCM transient climate change experiments. *J. Climate,* **16,** 1573–1582.

Stommel, H., and A. B. Arons, 1960: On the abyssal circulation of the world ocean—II. *Deep-Sea Res.,* **6,** 217–233.

Sun, S., and R. Bleck, 2001: Atlantic thermohaline circulation and its response to increasing CO_2 in a coupled atmosphere–ocean model. *Geophys. Res. Lett.,* **28,** 4223–4226.

Trenberth, K. E., and J. M. Caron, 2001: Estimates of meridional atmosphere and ocean heat transport. *J. Climate,* **14,** 3433–3443.

Tziperman, E., 2000: Uncertainties in thermohaline circulation response to greenhouse warming. *Geophys. Res. Lett.,* **27,** 3077–3080.

Wallace, J. M., and Coauthors, 2000: *Reconciling Observations of Global Temperature Change.* National Academy Press, 85 pp.

Wiebe, E. C., and A. J. Weaver, 1999: On the sensitivity of global warming experiments to the parameterisation of sub-grid scale ocean mixing. *Climate Dyn.,* **15,** 875–893.

Wood, R. A., A. B. Keen, J. F. B. Mitchell, and J. M. Gregory, 1999: Changing spatial structure of the thermohaline circulation in response to atmospheric CO_2 forcing in a climate model. *Nature,* **399,** 572–575.

Yao, M. S., and A. D. Del Genio, 2002: Effects of cloud parameterization on the simulation of climate changes in the GISS GCM. Part II: Sea surface temperature and cloud feedbacks. *J. Climate,* **15,** 2491–2503.